Coverage Dependent Molecular Assembly of Anthraquinone on Au(111)

Andrew S. DeLoach[1], Brad R. Conrad[2,*], T.L. Einstein[3], and Daniel B. Dougherty[1]

1. Department of Physics, North Carolina State University, Raleigh, NC 27695-8202

2. Department of Physics and Astronomy, Appalachian State University, Boone, NC 28608

3. Department of Physics & CMTC, University of Maryland, College Park, MD 20742-4111

Corresponding Author: dbdoughe@ncsu.edu

Abstract: A scanning tunneling microscopy (STM) study of anthraquinone (AQ) on the Au(111) surface shows that the molecules self-assemble into several structures depending on local surface coverage. At high coverages a close-packed saturated monolayer is observed while at low coverages, mobile surface molecules coexist with stable chiral hexamer clusters. At intermediate coverages, a disordered 2D porous network interlinking close-packed islands is observed in contrast to the giant honeycomb networks observed on for the same molecule on Cu(111). This difference verifies the predicted extreme sensitivity (Wyrick *et al., Nano Letters 11*, 2944 (2011),.) of the pore network to small changes in surface electronic structure. Quantitative analysis of the 2D pore network reveals that the areas of the vacancy islands are distributed log-normally. Log-normal distributions are typically associated with the product of random variables (multiplicative noise), and we propose that the distribution of pore sizes for AQ on Au(111) originates from random linear rate constants for molecules to either desorb from the surface or detach from the region of a nucleated pore.

*Present address: AIP, 1 Physics Ellipse, College Park, MD 20740

1. Introduction

The self-assembly of atoms and molecules on metal surfaces is thought to be a way of efficiently fabricating nanoscale structures and controlling interfacial properties. The past years have seen many examples of self-assembled networks stabilizing localized nanostructure formation and acting as a template for additional monolayer (ML) growth.[1, 2] Control of the self-assembly processes could lead to very complex nanostructures. However ,the numerous and complex interactions between adsorbates and the substrate limit the *a priori* design of such detailed structures[3]. Good examples of this are the DNA nucleobases on the Au(111) surface, where each molecule forms a very different network due to different interaction strengths and molecular geometry.[4-7]

Importantly, molecular assemblies on surfaces are not necessarily well-ordered. For example, recent studies of manganese phthalocyanine on Bi_2Te_3 show poor ordering,[8] cytosine on Au(111) shows a random pore network,[4] and second layers of diF-TES-ADT are disordered[9] despite ordering in the first layer. It is important to develop as much quantitative understanding of such disordered aggregates as possible. Furthermore, disorder at or near metal-organic interfaces may have significant implications for the efficiency of charge injection.[10, 11] In addition to the practical value of quantifying structural disorder, molecular adsorbates provide an intriguing opportunity in basic statistical physics of complex systems to connect microscopic interactions with larger-length-scale statistical properties.

Anthraquinone (AQ), and relatedly pentacenequinone, have been shown to make unusually large, porous, highly regular 2D surface structures on Cu(111)[12] driven microscopically by a combination of weak hydrogen bonding and subtle substrate-assisted interactions.[13] The latter interactions were found to be extremely sensitive to energetic shifts in the metallic surface state

due to charge transfer to the adsorbate.[13] To this end it is of interest to characterize the behavior of AQ on Au(111), which is very similar to Cu(111) but with small differences in surface crystallography and surface state electronic properties.[14] These small differences allow a direct experimental test of the predicted sensitivity of pore network formation to substrate details.[13] A previous study of AQ/Au(111) showed spatially-ordered and close-packed islands interlinked by a disordered porous "chevron" network on the Au(111) surface.[15] As on Cu, the pore sides are made up of AQ chains that form due to weak hydrogen bonding between the carbonyl oxygen atoms and the aromatic hydrogen atoms on neighboring molecules.

A major motivation of the present paper is to focus attention on the origin and quantitative statistical properties of the disordered pore network of AQ on Au(111). The fact that a disordered, rather than an ordered, pore network is found for AQ on Au(111) is important when contrasted with the high order of the dramatic regular giant honeycomb pore network observed on Cu(111).[12, 13] The ordering in that system is evidently quite delicate, requiring a narrow range of coverages. The presented observations support this by showing that only modest changes in substrate electronic structure and processing conditions destroy long-range pore ordering.

In what follows, we present observations of several new AQ surface assemblies on Au(111) over a range of surface coverages in addition to our quantitative analysis of the disordered pore network. We identify a new close-packed ordered structure of AQ on Au(111) different from observations in previous reports[15] as well as stable chiral hexameric clusters at very low coverage. A major goal is to develop some degree of quantitative understanding of disordered molecular network formation on surfaces. For this reason, we focus significant attention on the disordered structures of AQ on Au(111). We infer that random walk motion of the vacancy islands and random vacancy coalescence encourages disordered networks as seen in other systems.[16-18] The

statistical distribution of AQ pore sizes is found to be well fit by a log-normal function. This fact is attributed to the random multiplicative nature of the vacancy island formation within the perspective of vacancy attachment kinetics following a "law of proportionate effect."[19, 20] We hypothesize that similar generic physical models are likely to underpin the statistical properties of other disordered aggregates.[4]

2.Experimental Methods

Two Au(111) substrates, a thermally deposited Au(111) thin film on mica and a single Au(111) crystal, were used for this study, though no differences are expected or observed between these two substrates. The substrates were cleaned using multiple 1 hr Ar^+ sputtering and 700 K annealing cycles, then confirmed to be atomically clean by STM imaging before molecule deposition. Imaging was conducted in constant-current mode using tungsten tips, and image calibration was accomplished using the known dimensions of the herringbone reconstruction.[9] The substrates were prepared in UHV, with a base pressure of ~3 x 10^{-11} Torr, housing a commercial variable-temperature STM, Omicron VT-XA, connected by a gate valve to a separate organic deposition chamber. AQ was loaded as received (Sigma-Aldrich) into a glass ampoule sealed to a high-vacuum flange differentially pumped (to ~5 × 10^{-7} Torr) behind a gate valve separating it from the deposition chamber. Several layers of AQ molecules were deposited in the organic deposition chamber (base pressure 5 × 10^{-8} Torr) by heating the powder in the ampoule using an external heating tape and opening the gate valve. Typical temperatures of the ampoule were ~350K and the organic deposition chamber rose to ~2 × 10^{-6} Torr during deposition, dominantly due to the anthraquinone vapor. This dosing procedure and chamber setup has been used in the past to adsorb small molecules in highly ordered phases onto the reactive Cu(110) surface.[21] The substrates were held at room temperature during a short (~ 10 s) deposition and then annealed to

~400 K for 30 minutes to desorb AQ molecules from multilayers. After creating monolayer coverages by desorption, the samples were cooled to ~130 K for STM imaging.

3.Results and Discussion

3.A High Density: brickwork ordered structure

The close-packed structure of AQ on Au(111) on mica at a coverage approaching a ML can be seen in Figure 1a and the close up, Figure 1b. The well-known herringbone reconstruction of Au(111) is evident through the molecular layer of Figure 1a. Individual AQ molecules can be resolved in this close-packed ML and are seen to self-assemble into a brickwork pattern illustrated in Figure 1b, as is common in related molecular systems of benzene,[22, 23] naphthalene and anthracene,[23] and pentacene.[24] The close-packed lattice constants are measured to be **a** = 1.08 nm

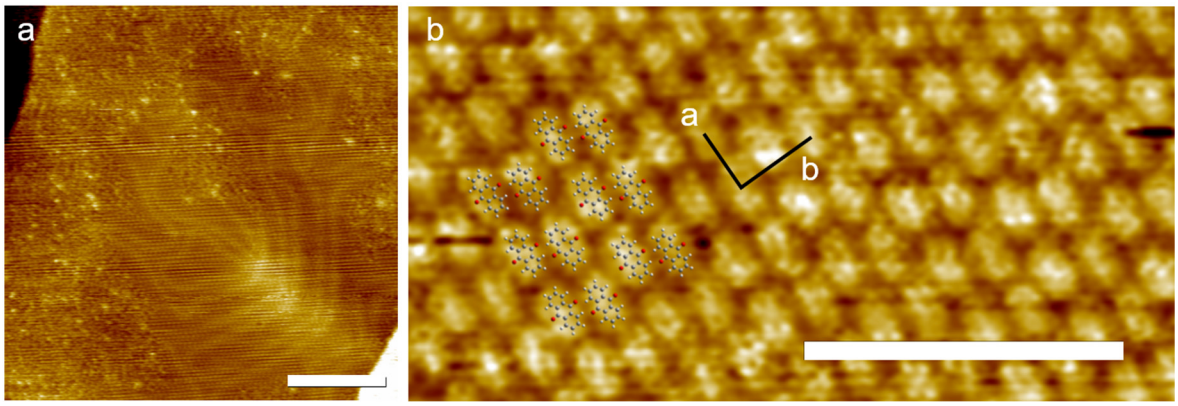

Figure 1: a) An (80 nm)^2 STM image of AQ deposited onto a cleaned Au(111) on mica substrate. V = + 0.5 V, I = 20 pA, scale bar is 20 nm; b) A (12 x 6) nm^2 close up of the AQ monolayer with an overlaid illustration of the suggested molecular structure observed for the close packed structure. Scale bar is 5 nm. Lattice constants are measured to be **a** = 1.08 nm and **b** = 1.34 nm and **γ** = 85.87°. Images was taken at V = + 0.5 V, I = 20 pA.

and **b** = 1.34 nm, and γ = 85.9°, which are similar to the related ML system of 6,13-dichloropentacene on Au(788).[25] The corresponding molecular density of 1.38 molecules/nm^2 defines what we consider the saturated ML in the AQ/Au(111) adsorption system. Kim *et al*. reported anthraquinone close-packed structures with distinct packing structures.[15] They primarily observed a square close-packed structure with a molecular density of 1.10 molecules/nm^2 after they dosed at 150K. When the sample was annealed to room temperature, the dominant structure shifted to a chevron structure with density 1.34 molecules/nm^2. The ML presented here was obtained by depositing more than a ML and then lightly annealing to desorb excess molecules, leaving behind the brickwork structure observed. As the annealing temperature is increased, the molecular-bond density also increases, and the ML becomes more stable due to more molecular bonds per unit cell.

The visible herringbone reconstruction indicates that the soliton walls do not interfere with the formation of the brickwork close-packing. In Figure 1a, it can be seen that there are regions of disorder coexisting with the ordered brickwork regions. These disordered regions are due to a lower local molecule density and high molecular mobility on the Au(111) surface. Thus, the molecules do not lock into a brickwork pattern at this local coverage, but rather adopt different in-plane orientations and adsorption locations. While not modifying the crystallization of the brickwork structure at high local coverage, the Au(111) herringbone soliton walls become relevant in the sub-ML regime as they apparently act to bound the regions of order and disorder.

3.B Low-Density: Stable Chiral Hexamers

An (80 nm)^2 STM image of AQ on Au(111) film on mica is shown in Figure 2a. At low coverages of AQ molecules, a low density molecular gas bound by the soliton walls of the herringbone reconstruction is observed. The blurred nature of the large regions of the STM images

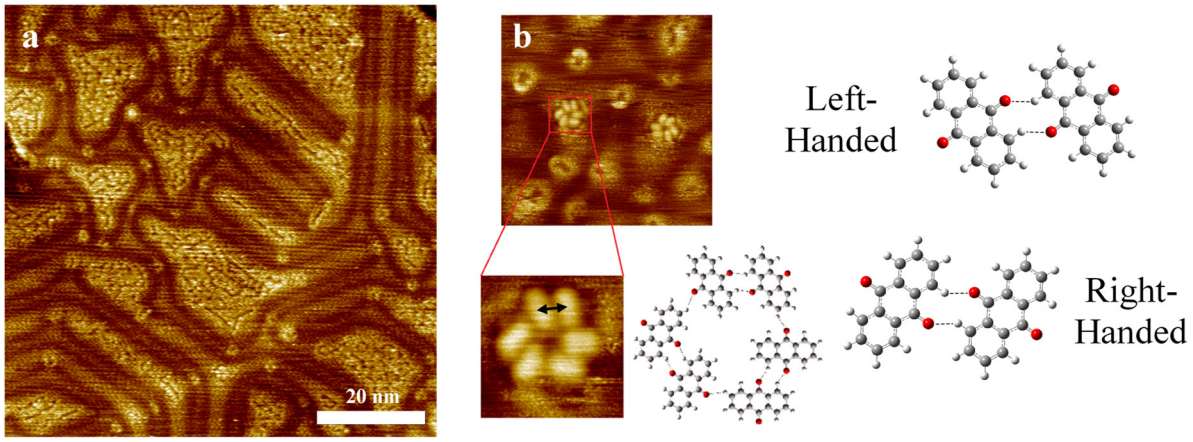

Figure 2: a) An (80 nm)^2 STM image of a low density AQ gas being bound by Au(111) soliton walls. b) A (20.2 nm)^2 STM image of the nanostructures that forms within herringbone domains with an enlarged, (6.54 nm)^2 STM image of the chiral structure. Also, molecular arrangements of the left and right-handed dimer pairs, with the dotted lines representing weak hydrogen bonding. Three pairs of left-handed or right-handed dimers give rise to a pinwheel structure that maintains the chirality, as observed in Figure 1b. Images (a) and (b) were taken with tip bias of + 0.5 V and tunneling current I = 20 pA.

in Figure 2a and 2b indicate that the AQ molecules are mobile on the surface at this temperature. This agrees with other reports for comparable systems of small molecule adsorbates with relatively weak intermolecular interactions.[26, 27] However, since the soliton walls constrain molecular motion, AQ molecules can collect at higher local densities within the larger fcc domains of the Au(111) surface. At these locations stable disordered islands and pinwheel structures are observed to form randomly, as seen in Figure 2b.

The observed pinwheel structure is formed by three dimer pairs bound together with three-fold symmetry. The outer sides measure (1.9 ±0.1) nm with a (60 ± 2)° angle between sides. The

spacing between AQ molecules in each dimer measure (0.81 ± 0.02) nm, as indicated in the zoomed-in portion of Figure 2b by the double-headed arrow. Hydrogen bonding between the central-ring oxygen atoms and the hydrogen termination likely drive structure formation at this density, as has been seen in other systems.[28] These regularly-shaped pinwheel structures are observed to have two chiral conformations, due to the constituent dimer pairs also being chiral, as seen in Figure 2b. There is no apparent chirality preference: both clockwise and counterclockwise pinwheels occur with comparable probability on large substrates in our observations.

Chiral hexamers of AQ on Au(111) join the ranks of several known stable molecular surface clusters that occur at low average surface density. For example, nitro-napthalene forms a racemic surface mixture of stable decamer clusters on Au(111).[29] Rubrene makes a range of stable clusters on Au(111) from dimers up to aggregates of pentamers,[30] and large chiral aggregates.[31] Carbon monoxide adsorbates on Au(111) can be found forming a similar range of stable clusters at very low temperature.[32] The prevalence of stable supramolecular clusters in this diverse class of adsorbates is significant since it could provide approaches to creating structural diversity in assemblies. If cluster precursors can be stabilized by assembly conditions such has temperature and surface coverage, then structural properties of clusters might propagate in a controlled fashion across length scales.

3.C Intermediate Coverage: Disordered Pore Network

At ~0.65 ML surface coverage, disordered islands are observed with an amorphous pore network linking neighboring islands, as shown in Figure 3a. Close examination reveals that the sides of the pores are formed from chains of AQ molecules, similar to reports of a "chevron structure" in a previous study.[15] In this section, we go beyond a simple description of the network by connecting its existence to scenarios with multiple weak hydrogen bonds and predictions about

the extreme sensitivity of giant honeycombs predicted theoretically.[13] In the next section, we also provide a physical mechanism that explains the quantitative pore-size distribution extracted from our observations.

The disordered network does not have any registry with the substrate symmetry directions, and the Au(111) herringbone reconstruction does not appear to have any influence, indicating that the interaction with the substrate is weak. The amorphous network here is more characteristic of a

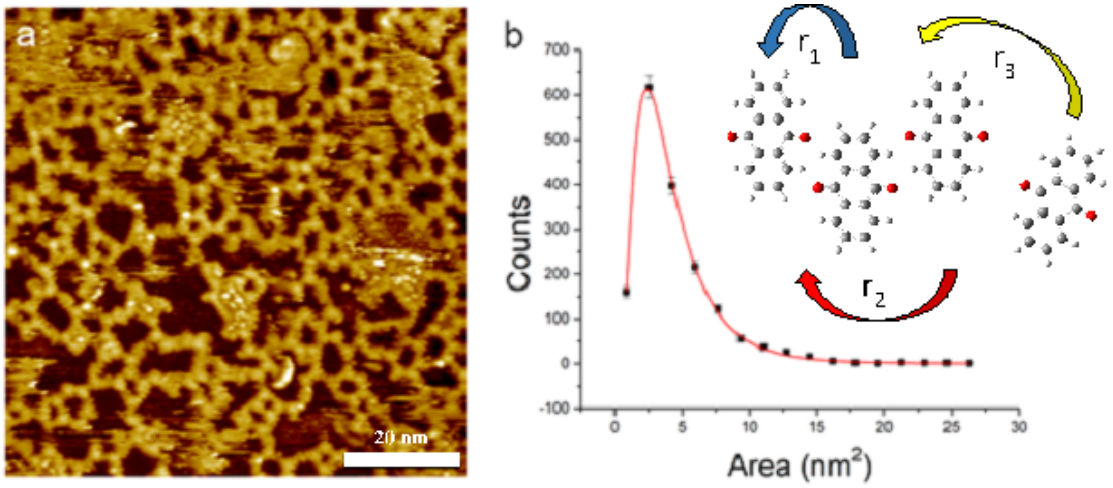

Figure 3: a) A (80 nm)^2 STM image of AQ on Au(111) on mica displaying disordered close packed islands with linking chains. Scale bar is 20 nm. Image was taken at tip bias +2.0 V and tunneling current I = 15 pA; b) A histogram of the distribution of pore areas taken from 31 images with a total of 1664 counts. The red solid line represents a log-normal distribution with fitting parameters discussed in the text. Inset of b): An illustration of possible chain formation via the addition of AQ molecules to an existing AQ chain. The pore area growth rate is related to the various molecular attachment (and detachment) rates r_n In the inset of Figure 3b, different plausible AQ molecular attachment rates are represented schematically as different colored arrows.

2D glass-like molecular network, similar to that seen for cytosine on Au(111)[4] or cobalt with dicarbonitrile linkers on Au(111) or Cu(111).[33]

As previously mentioned, the lack of order in the intermediate porous coverage regime of AQ on Au(111) is in stark contrast with the long-range ordering seen for AQ pores on Cu(111). Several factors can contribute to the origin of this difference including the surface electronic structure of Au(111), the temperature of observation, trace impurities, or the desorption process used to create AQ aggregates in our work. While we will not make a definitive statement about which of these several factors is involved in preventing pore ordering, we will address each in turn and argue that electronic structure effects are the most significant.

The influence of the electronic structure of the surface state of Au(111) is the most interesting to consider since the related surface state of Cu(111) plays a major role in stabilizing large AQ pores on that surface.[12, 13] The Shockley surface state on Au(111) is very similar to that on Cu(111): ARPES measurements give the value of E_F-E_0 where E_0 is the minimum of the surface-state parabola, as 0.435eV for Cu and 0.487 eV for Au,[34] However, their effective masses differ considerably: 0.255 for Cu and 0.412 for Au, in units of free electron mass.[34] (Correspondingly, the Fermi wavelength is about 2.9 nm for Cu and 3.6 nm for Au..[14,34])

Even these relatively small differences can be sufficient to destroy the stability of the unique large pores, according to the computational study in Wyrick et al. for AQ on Cu(111).[13] They found that the very small surface-state binding energy modification of only ~ 30 meV that occurs upon adsorption of an appropriate coverage of AQ on Cu(111) is *essential* to create the closed-shell pore electronic structure that stabilizes the ordered network. Even small deviations ruin the closed-shell "pseudo-atom" structure of the pores and destabilize the network. For a 2D free-electron gas the number of electrons per area is m_{eff} (E_F-E_0)/($\pi \hbar^2$). Hence, assuming E_F = 0

as is conventional in ARPES graphs, the ratio of the number of electrons in a honeycomb pore for gold to that for copper is $(m_{eff}^{Au}/m_{eff}^{Cu})\ |E_0^{Au}/E_0^{Cu}|\ (a^{Au}/a^{Cu})^2$. The lattice constants are well known. With the ARPES values for clean surfaces, this ratio is about 0.885. This is just a zeroth estimate, since charge transfer between AQ and the substrate produces a non-negligible shift in E_0, reducing $|E_0^{Cu}|$ by nearly 0.02 meV for AQ on Cu(111) at the concentration of the honeycomb; the corresponding shift on Au(111) is unavailable without extensive ARPES measurements. (The effective mass should also change, but only by a quarter the energy shift.[35]) Evidently, AQ/Au(111) misses the stringent conditions identified by Wyrick et al.,[13] presumably due to the different Shockley surface state properties (effective mass and band bottom) on the two surfaces. Corrections for charge transfer are likely to make the ratio even smaller, since for AQ/Cu it decreases $|E_0^{Cu}|$ (by ~7%) while $|E_0^{Au}|$ would need to increase to overcome the mall value of $m_{eff}^{Au}/m_{eff}^{Cu}$. Alternate adsorbates with enhanced charge transfer with Au(111) could conceivably result in larger changes[35] to give rise to a similar pore electron occupation as for AQ/Cu(111) but it would be astonishing if such adsorbates could replicate the delicate intermolecular interactions needed to form the chains and vertices of the honeycomb. Thus, the small electronic structure differences between Au(111) and Cu(111) surface states are sufficient to drastically modify pore formation conditions for AQ on Au(111) since they are already larger than the differences identified by Wyrick et al.[13] Indeed, our observations suggest that there is no stable pore network whatsoever on Au(111). Direct spectroscopic measurements of the adsorption-induced electronic structure would be of value in modeling the substrate-induced effects in this system. A more extreme change would be to consider AQ adsorption on Ag(111), which has a Shockley surface state with parabolic minimum at only ~ 80 meV below the Fermi level[14] and would thus be expected to preclude ordered AQ pore networks. While no observations of AQ assembly on

Ag(111) exist to date, a related system of TCNQ on Ag(111) shows a disordered pore network[36] that is qualitatively similar to the one found in this work for AQ/Au(111).

It is also possible that the imaging temperature or the desorption process used to create disordered networks shown in Figure 3a prevent ordering. One might view the network as a thermally-disordered (at 130 K) variant of the related ordered pore network visualized at liquid helium temperatures on Cu(111), although once formed the ordered pore network pattern persisted up to 200K.[12] This would suggest that at liquid helium temperatures the AQ pore network on Au(111) would be ordered, a hypothesis that we cannot currently test. Alternatively, one might view the disordered network as a structure that is kinetically trapped during the complex desorption process employed to create monolayer structures. Neither of these contributions to the origin of disorder can be ruled out completely, but given the connection made above to the delicate electronic structure contributions known for AQ on Cu(111),[13] we favor assigning electronic structure differences as the most significant factor. Also worth noting is that AQ network on Cu(111) only occurs in a narrow coverage regime. At lower coverages, AQ molecules just form long chain across the surface[37] and at higher coverages it is observed that close-packed AQ islands form that are surrounded by the hexagonal AQ network[13]. This indicates that even at higher coverages a uniform network can form sufficiently far away from islands where the local coverage is closer to that of the ideal coverage for the hexagonal network. Since we do not observe any ordering of AQ on Au(111) even far from islands, we can be more confident that the difference in electronic structure is the most significant factor. In the next section, we propose a quantitative model for the observed pore size distribution without reference to the surface state since it does not play a large role in network development in the AQ on Au(111) system.

3.D Statistical Distribution of Pore Sizes

To quantify the statistical properties of the observed pore network, the pore detection feature of SPIP (v. 5.1.5) image analysis software was used to measure the areas of each pore. Filters were used in order to exclude any irregularly shaped pores, noise, and pores cut off by the edge of the image (as these would affect the resulting pore distribution). A total of 1664 pores from 31 images were measured, and the resulting distribution of pore areas was observed to be well represented by a 2-parameter (since the offset is 0) log-normal distribution $f(x)$[19, 20, 38-40]

$$f(x) = \frac{a}{\sqrt{2\pi}\sigma x} exp\left[-\frac{\left(ln\left(\frac{x}{x_\mu}\right)\right)^2}{2\sigma^2}\right], \quad (1)$$

where x is the pore area and x_μ is exp (μ), where μ is the mean of ln x both being measured in in the same units, in this case nm^2, along with the other lengths in Eq. (1), thus avoiding in standard fashion[38, 40, 41] concerns about a dimensional argument of the logarithm; σ is the standard deviation of ln x, , and a is a constant with dimensions of area (total counts × bin size, here 1.7 nm^2). The fitted histogram can be seen in Figure 3b. The best-fit values of the three fitting parameters are: μ is 1.276 ± 0.015; σ is 0.634 ± 0.009; and a, the amplitude or total pore area (since the log-normal distribution f is normalized), is (2851 ± 81) nm^2. Thus, the characteristic pore area, x_μ, is (3.58 ± 0.05) nm^2 [the mean area, exp (μ + σ^2/2), is 4.37 nm^2]. These characteristic sizes are smaller than the size of the highly regular pore network reported on Cu(111), where pores have areas ~9.6 nm^2.[13] The value exp(σ) ≈ 1.9 is modestly larger than the values ~ 1.3 found for metal nanoparticles with a log-normal size distribution and so is regarded as reasonable.[39]

Log-normal distributions are associated with a multiplicative product of many independent random variables (becoming apparent after just four sequential stochastic events[41]) and have been observed in the size distributions of nanoparticles and in other diverse materials systems.[38, 39, 42, 43]

Here, a model is proposed to link the growth kinetics of the AQ 2D pore network to the observed log-normal distribution and thus qualitatively explain the shape of the distribution of pore areas. It is well known that two-dimensional vacancy islands can migrate across surfaces due to thermal fluctuations.[44] This occurs due to adatoms travelling around the periphery of the vacancy island step edge or detaching and travelling via a thermally driven random walk to another part of the step edge.[18, 45, 46] The complex collective motions give rise to a random walk for the entire vacancy island across the surface.[18, 45, 46] Furthermore, adatom islands and vacancy islands can also coalesce into larger islands.[16, 17] Considering these random diffusion and aggregation processes in the observed 2D AQ network on Au(111), we can generate a specific phenomenological model of the origin of the log-normal distribution.

The kinetics of pore formation is modeled phenomenologically by vacancy (or vacancy island) attachment to an existing pore according to the "law of proportionate effect".[19, 20] This law posits that the increase in pore area from one growth step to the next is proportional to the current area of the pore, which in the continuum limit is simply first-order kinetics. The pore area is required to appear in our model of the data in Figure 3b and can be justified by the fact that our experiments are in a regime of both vacancy diffusion and direct desorption from the surface. The mechanisms by which a pore grows during a growth step are vacancy attachment or molecule desorption during annealing and the coalescing of neighboring vacancy islands facilitated by the random walk motion of the islands. As a recursion relation the kinetics of pore area growth can be expressed as:

$$A_j - A_{j-1} = k_j A_{j-1} \quad , \qquad (2)$$

where A_j represents the pore area at growth step j and k_j is a *random* rate constant describing the rate of growth at the j^{th} step. This leads to an area after n iterations that is given by,

$$A_n = A_0 \prod_{j=1}^{n} (1 + k_j). \qquad (3)$$

From this expression, where A_0 is the initial increment of area created upon pore nucleation, it is evident that the pore area is proportional to a product of random variables. This is exactly the condition required to result in a log-normal statistical distribution after a sufficiently long pore growth time. In the case of AQ pores on Au(111), Eq. (3) provides a plausible identification of the relevant multiplicative random variables as the random attachment rate of vacancies and the subsequent diffusion and aggregation of vacancy island clusters. The possibility that these rates can be random variables (as opposed to fixed rate constants) is supported by the possibility of several different weak-hydrogen bonding interaction geometries indicated in the inset of Figure 3b and by the strong possibility of complex cooperative motions within a vacancy island. Importantly, the phenomenological model described here has the primary goal of explaining the log-normal shape of the distribution in a well-developed pore network where the number of increments of Eq. (3) is large. It is not a mechanistic model of the kinetic evolution of pore geometry over time such as those used to describe vacancy cluster evolution on metal surfaces.[47]

The model encoded in Eqs. (2) and (3) describes growth in pore area under desorption conditions where the total number of molecules on the surface is not conserved (note that this general model could also apply to direct growth of the network by deposition). Within this model, pore size grows with time during the desorption process, resulting in a shift in the maximum of the log-normal distribution. Such a quantitative picture should be generic enough to test by applying the same ideas to the numerous disordered porous molecular assemblies known to date.[4, 36] Another important test would be to follow the evolution of pore-size distribution; the results would clarify the scaling of the pore size distribution but might be difficult to obtain in practice if the coverage window where disordered pores exist is not large. Finally, we note that kinetic Monte Carlo

simulations of pore networks would be very valuable if reasonable estimates for relevant vacancy attachment rates could be made. These could in principle be estimated from first principles calculations of the adsorption structures described here and is a worthy topic of future computational research. However, this project would face a significant challenge due to the weak intermolecular interactions and the multiplicity of interactions for different orientations of the AQ molecules. Furthermore, uncertainty about the size and microscopic origin of relevant barriers can lead a vast diversity of possible surface phenomena in KMC simulations, especially when one must make uncontrolled approximations to achieve a computationally-feasible model.[48, 49] Obtaining compelling results would be daunting. The phenomenology embodied in Eq. (3) provides significant conceptual understanding applicable to other systems even in the absence of more detailed microscopic models.

4. Summary and Conclusions

In summary, we report coverage-dependent STM studies on AQ on Au(111) aimed at clarifying the diversity of surface structures in a system where numerous relatively weak intermolecular and molecule-substrate interactions can operate. We observed a new ordered structure of AQ on Au(111) that is different from those previously reported.[15] In addition, at very low coverages, we observed unexpected stable hexamers that form chiral rings on the surface, seeded by the underlying chirality of weak-hydrogen-bonded dimers. Finally, we quantified the statistical properties of a disordered pore network of AQ on Au(111) that is very different from the highly ordered pore network seen for the same molecule on Cu(111).[13] The microscopic origin of this difference is ascribed to the different surface state electronic structure on Au(111) compared to Cu(111) that does not allow the delicate "closed shell" electronic stabilization operative for AQ/Cu(111).[13] In the disordered network, the pore sizes can be described by a log-normal

statistical distribution. This particular form leads us to suggest a quantitative phenomenological model in which a product of random vacancy attachment rates determines pore size according to a first order kinetic model. We expect that this model is generic enough to apply with small modification to other related networks and may also provide guidance in explaining underlying mechanisms in other physical systems involving log-normal distributions. Given the increasing prevalence of disorder at molecular interfaces,[4, 9] it is important to strengthen our quantitative statistical understanding of complex structures such as we describe here.

5.Acknowledgements:

This work was supported in part by NSF Grant No. CHE 13-05892.

6.References

1. J. A. Theobald, N. S. Oxtoby, M. A. Phillips, N. R. Champness and P. H. Beton, Nature **424** (6952), 1029-1031 (2003).
2. D. Kühne, F. Klappenberger, W. Krenner, S. Klyatskaya, M. Ruben and J. V. Barth, Proceedings of the National Academy of Sciences **107** (50), 21332-21336 (2010).
3. J. V. Barth, Annual Review of Physical Chemistry **58** (1), 375-407 (2007).
4. R. Otero, M. Lukas, R. E. A. Kelly, W. Xu, E. Laegsgaard, I. Stensgaard, L. N. Kantorovich and F. Besenbacher, Science **319** (5861), 312-315 (2008).
5. R. E. A. Kelly, W. Xu, M. Lukas, R. Otero, M. Mura, Y.-J. Lee, E. Lægsgaard, I. Stensgaard, L. N. Kantorovich and F. Besenbacher, Small **4** (9), 1494-1500 (2008).
6. R. Otero, M. Schöck, L. M. Molina, E. Lægsgaard, I. Stensgaard, B. Hammer and F. Besenbacher, Angewandte Chemie International Edition **44** (15), 2270-2275 (2005).
7. W. Xu, R. E. A. Kelly, R. Otero, M. Schöck, E. Lægsgaard, I. Stensgaard, L. N. Kantorovich and F. Besenbacher, Small **3** (12), 2011-2014 (2007).
8. P. Sessi, T. Bathon, K. A. Kokh, O. E. Tereshchenko and M. Bode, Nano Letters **14** (9), 5092-5096 (2014).
9. S. M. Huston, J. Y. Wang, M. A. Loth, J. E. Anthony, B. R. Conrad and D. B. Dougherty, J. Phys. Chem. C **116** (40), 21465-21471 (2012).
10. M. A. Baldo and S. R. Forrest, Physical Review B **64** (8), 085201 (2001).
11. A. L. Burin and M. A. Ratner, Journal of Polymer Science Part B: Polymer Physics **41** (21), 2601-2621 (2003).
12. G. Pawin, K. L. Wong, K. Y. Kwon and L. Bartels, Science **313** (5789), 961-962 (2006).
13. J. Wyrick, D. H. Kim, D. Z. Sun, Z. H. Cheng, W. H. Lu, Y. M. Zhu, K. Berland, Y. S. Kim, E. Rotenberg, M. M. Luo, P. Hyldgaard, T. L. Einstein and L. Bartels, Nano Letters **11** (7), 2944-2948 (2011).
14. F. Reinert, G. Nicolay, S. Schmidt, D. Ehm and S. Hufner, Physical Review B **63** (11), 115415 (2001).

15. J. Y. Kim, W. J. Jang, H. Kim, J. K. Yoon, J. Park, S.-J. Kahng, J. Lee and S. Han, Applied Surface Science **268**, 432-435 (2013).
16. M. Eßer, K. Morgenstern, G. Rosenfeld and G. Comsa, Surface Science **402–404**, 341-345 (1998).
17. J. M. Wen, J. W. Evans, M. C. Bartelt, J. W. Burnett and P. A. Thiel, Physical Review Letters **76** (4), 652-655 (1996).
18. K. Morgenstern, G. Rosenfeld, B. Poelsema and G. Comsa, Physical Review Letters **74** (11), 2058-2061 (1995).
19. J. Aitchison and J. A. C. Brown, *The Lognormal Distribution*. (Cambridge University Press, Cambridge, U.K., 1973).
20. D. B. Siano, Journal of Chemical Education **49** (11), 755-757 (1972).
21. A. Pronschinske and D. B. Dougherty, Journal of Physical Chemistry Letters **1** (17), 2613-2617 (2010).
22. E. C. H. Sykes, P. Han, S. A. Kandel, K. F. Kelly, G. S. McCarty and P. S. Weiss, Accounts Chem. Res. **36** (12), 945-953 (2003).
23. L. J. Wan and K. Itaya, Langmuir **13** (26), 7173-7179 (1997).
24. C. B. France, P. G. Schroeder, J. C. Forsythe and B. A. Parkinson, Langmuir **19** (4), 1274-1281 (2003).
25. J. Wang, I. Kaur, B. Diaconescu, J. M. Tang, G. P. Miller and K. Pohl, ACS Nano **5** (3), 1792-1797 (2011).
26. K. Y. Kwon, K. L. Wong, G. Pawin, L. Bartels, S. Stolbov and T. S. Rahman, Phys. Rev. Lett. **95** (16), 4 (2005).
27. K. L. Wong, G. Pawin, K. Y. Kwon, X. Lin, T. Jiao, U. Solanki, R. H. J. Fawcett, L. Bartels, S. Stolbov and T. S. Rahman, Science **315** (5817), 1391-1393 (2007).
28. M. Bohringer, K. Morgenstern, W. D. Schneider, R. Berndt, F. Mauri, A. De Vita and R. Car, Phys. Rev. Lett. **83** (2), 324-327 (1999).
29. M. Bohringer, K. Morgenstern, W. D. Schneider and R. Berndt, Angewandte Chemie-International Edition **38** (6), 821-823 (1999).
30. M. C. Blum, M. Pivetta, F. Patthey and W. D. Schneider, Physical Review B **73** (19) (2006).
31. M. C. Blum, E. Cavar, M. Pivetta, F. Patthey and W. D. Schneider, Angewandte Chemie-International Edition **44** (33), 5334-5337 (2005).
32. P. Maksymovych and J. T. Yates, Chemical Physics Letters **421** (4-6), 473-477 (2006).
33. M. Marschall, J. Reichert, A. Weber-Bargioni, K. Seufert, W. Auwarter, S. Klyatskaya, G. Zoppellaro, M. Ruben and J. V. Barth, Nat. Chem. **2** (2), 131-137 (2010).
34. P. Hyldgaard and T. L. Einstein, Europhys. Lett. **59** (2), 265-271 (2002).
35. K. Berland, T. L. Einstein and P. Hyldgaard, Physical Review B **85** (3), 035427 (2012).
36. C. Park, G. A. Rojas, S. Jeon, S. J. Kelly, S. C. Smith, B. G. Sumpter, M. Yoon and P. Maksymovych, Physical Review B **90** (12) (2014).
37. G. Pawin, University of California - Riverside, 2008.
38. C. G. Granqvist and R. A. Buhrman, Journal of Applied Physics **47** (5), 2200-2219 (1976).
39. L. B. Kiss, J. Soderlund, G. A. Niklasson and C. G. Granqvist, Nanostruct. Mater. **12** (1-4), 327-332 (1999).
40. S. J. Shaefer and L. Theodore, (CRC Press, Boca Raton, U.S.A., 2007).
41. W. R. Ott, Journal of the Air & Waste Management Association **40** (10), 1378-1383 (1990).
42. K. P. Gentry, T. Gredig and I. K. Schuller, Physical Review B **80** (17), 174118 (2009).
43. J. F. Shackelford and B. D. Brown, J. of Non-Crystalline Solids **44**, 379-382 (1981).
44. M. Giesen, Progress in Surface Science **68** (1–3), 1-154 (2001).
45. S. V. Khare, N. C. Bartelt and T. L. Einstein, Physical Review Letters **75** (11), 2148-2151 (1995).
46. S. V. Khare and T. L. Einstein, Physical Review B **54** (16), 11752-11761 (1996).

47. M. Giesen, Progress in Surface Science **68** (1-3), 1-153 (2001).
48. K. Kim and T. L. Einstein, Physical Review B **83** (24), 245414 (2011).
49. M. Simenas and E. E. Tornau, Journal of Chemical Physics **139** (15), 154711 (2013).

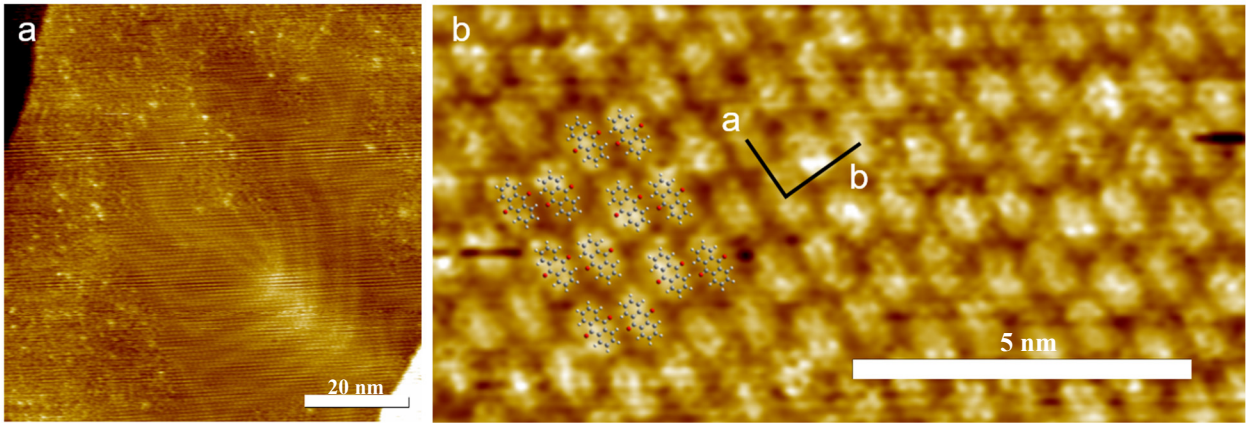

Figure 1: a) An (80 nm)^2 STM image of AQ deposited onto a cleaned Au(111) on mica substrate. V = + 0.5 V, I = 20 pA, scale bar is 20 nm; b) A (12 x 6) nm^2 close up of the AQ monolayer with an overlaid illustration of the suggested molecular structure observed for the close packed structure. Scale bar is 5 nm. Lattice constants are measured to be **a** = 1.08 nm and **b** = 1.34 nm and γ = 85.87°. Images was taken at V = + 0.5 V, I = 20 pA.

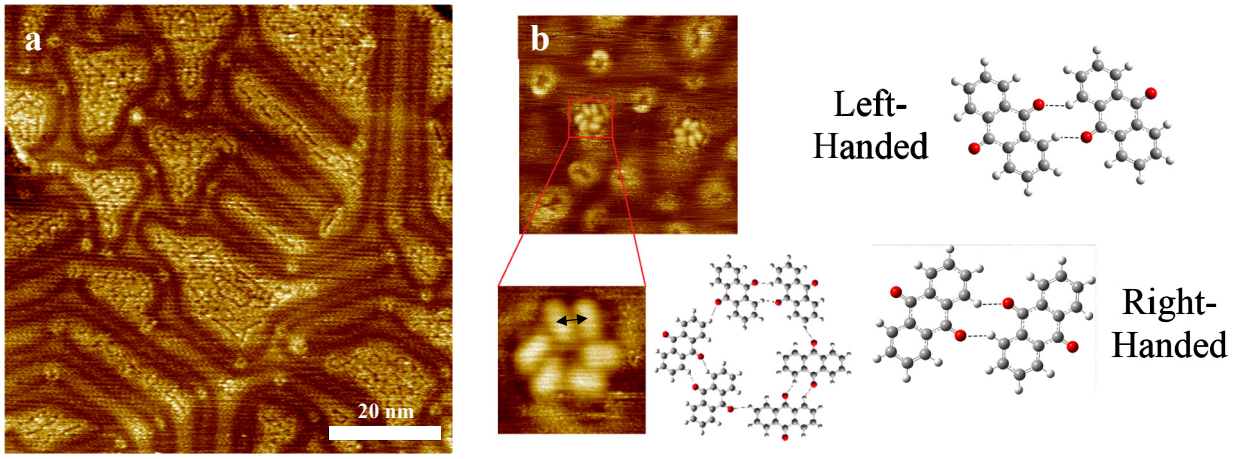

Figure 2: a) An (80 nm)^2 STM image of a low density AQ gas being bound by Au(111) soliton walls. b) A (20.2 nm)^2 STM image of the nanostructures that forms within herringbone domains with an enlarged, (6.54 nm)^2 STM image of the chiral structure. Also, molecular arrangements of the left and right-handed dimer pairs, with the dotted lines representing weak hydrogen bonding. Three pairs of left-handed or right-handed dimers give rise to a pinwheel structure that maintains

the chirality, as observed in Figure 1b. Images (a) and (b) were taken with tip bias of + 0.5 V and tunneling current I = 20 pA.

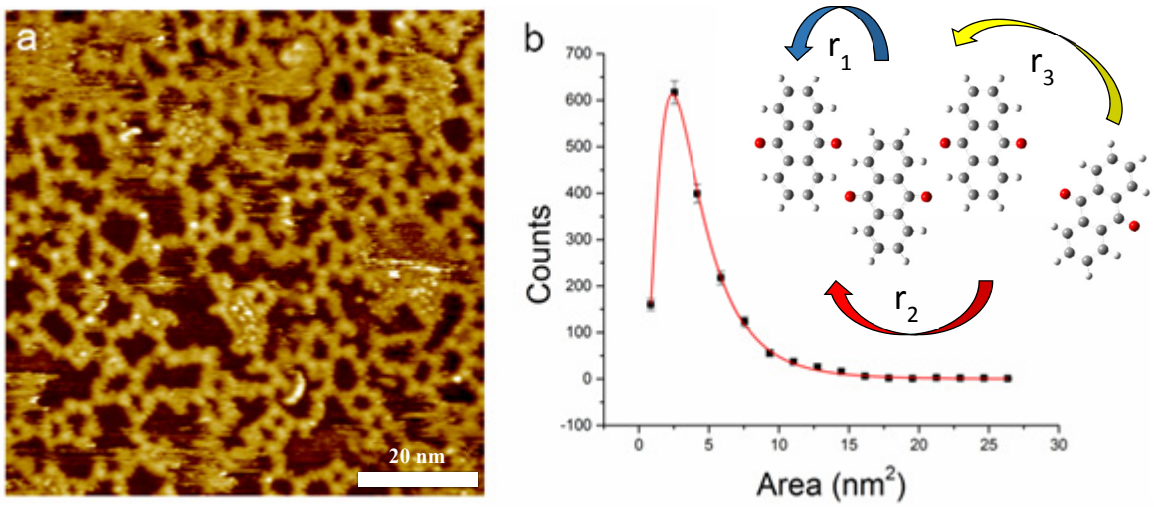

Figure 3: a) A (80 nm)^2 STM image of AQ on Au(111) on mica displaying disordered close packed islands with linking chains. Scale bar is 20 nm. Image was taken at tip bias +2.0 V and tunneling current I = 15 pA; b) A histogram of the distribution of pore areas taken from 31 images with a total of 1664 counts. The red solid line represents a log-normal distribution with fitting parameters discussed in the text. Inset of b): An illustration of possible chain formation via the addition of AQ molecules to an existing AQ chain. The pore area growth rate is related to the various molecular attachment (and detachment) rates r_n In the inset of Figure 3b, different plausible AQ molecular attachment rates are represented schematically as different colored arrows.

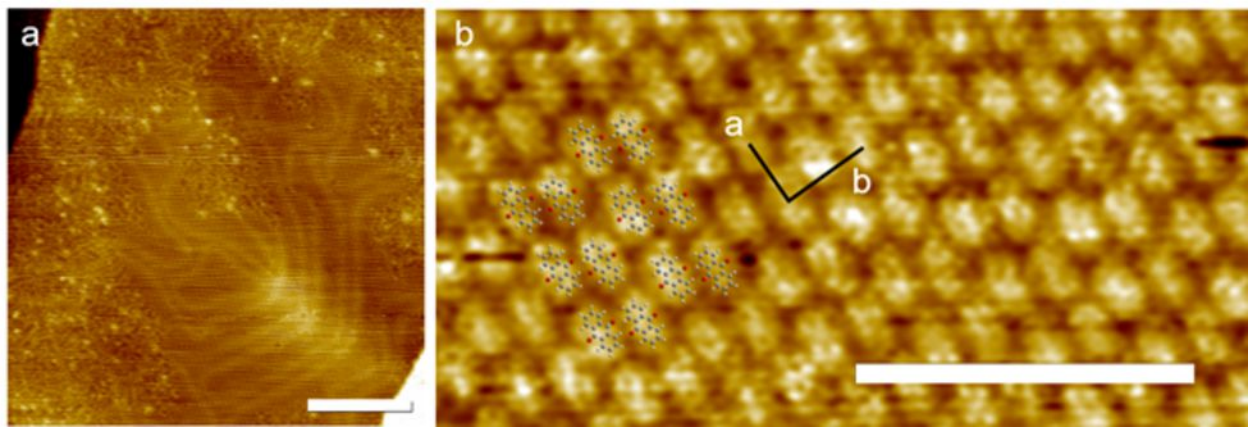
a
b
a
b

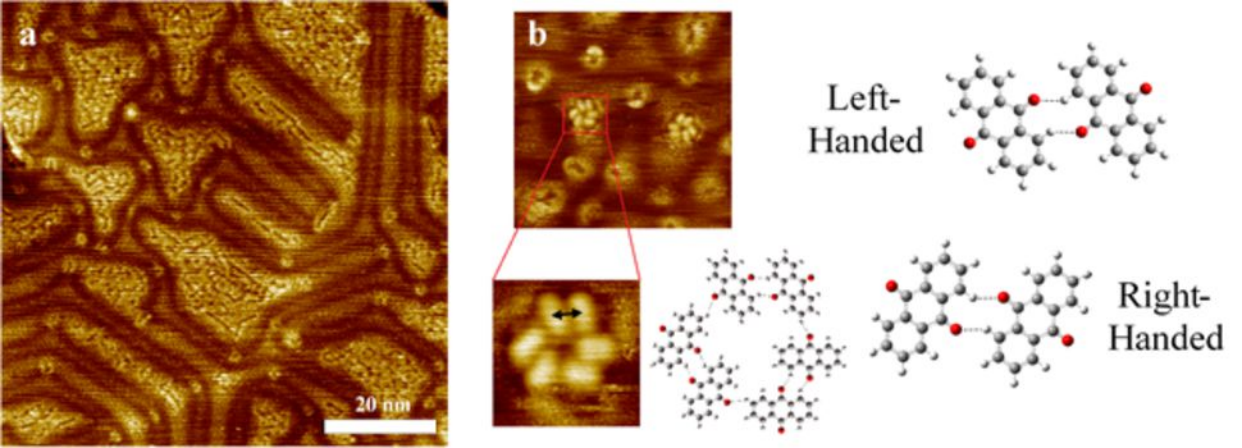
a
20 nm
b
Left-
Handed
Right-
Handed

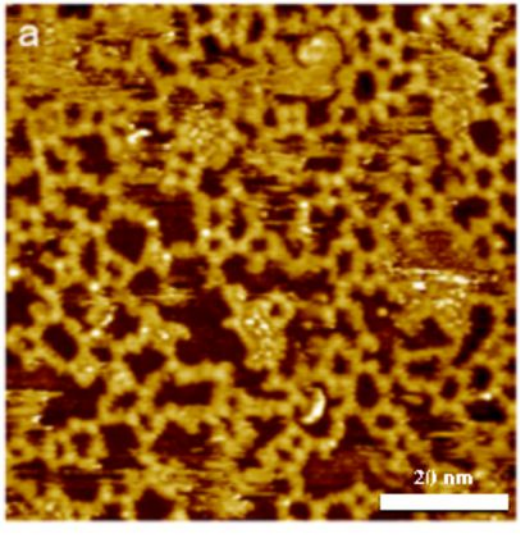
a
20 nm

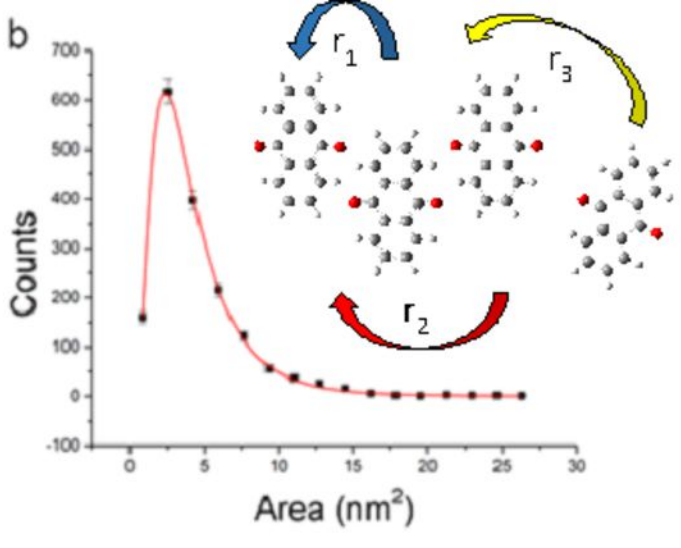
b
Counts
Area (nm²)
r1
r2
r3